Observation of quantum-limited spin transport in strongly interacting two-dimensional Fermi gases

C. Luciuk,[1] S. Smale,[1] F. Böttcher,[2] H. Sharum,[1] B. A. Olsen,[1] S. Trotzky,[1] T. Enss,[3] and J. H. Thywissen[1, 4]

[1]*Department of Physics, University of Toronto, Ontario M5S 1A7 Canada*
[2]*5. Physikalisches Institut and Centre for Integrated Quantum Science and Technology,*
Universität Stuttgart, D-70569 Stuttgart, Germany
[3]*Institut für Theoretische Physik, Universität Heidelberg, D-69120 Heidelberg, Germany*
[4]*Canadian Institute for Advanced Research, Toronto, Ontario M5G 1Z8 Canada*
(Dated: December 5, 2016)

We measure the transport and thermodynamic properties of two-dimensional ultracold Fermi gases through their demagnetization in a magnetic field gradient. Using a phase-coherent spin-echo sequence, we are able to separate bare spin diffusion from the Leggett-Rice effect, in which demagnetization is slowed by the precession of spin current around the local magnetization. We find that the bare transverse spin diffusivity reaches a minimum of $1.7(6)\hbar/m$, where m is the bare particle mass, when the two-dimensional scattering length is comparable to the inverse Fermi wave vector. Time-resolved spectroscopy during demagnetization reveals a thermodynamic transformation of the sample captured by the growth of the s-wave contact, whose steady state value gives only a 4% correction to the scale-invariant virial relation. The value of the contact is consistent with remaining predominantly in the upper energetic branch during demagnetization. Our observations support the conjecture that local relaxation rates in strongly interacting liquids are bounded from above by $k_B T/\hbar$.

Conjectured quantum bounds on transport appear to be respected and nearly saturated by quark-gluon plasmas [1, 2], graphene [3], bad metals [4, 5], and unitary Fermi gases [6–14]. For many modalities of transport these bounds can be recast as an upper bound on the rate of local relaxation to equilibrium $1/\tau_\mathrm{r} \lesssim k_B T/\hbar$, where k_B is the Boltzmann constant and T is temperature. Systems that saturate this bound can be considered "Planckian" [4, 5, 15], and do not have well defined quasiparticles promoting transport. A canonical example is quantum critical transport, where temperature provides the only scale. In this regime, one expects diffusivity $D \sim \hbar/m$, a ratio of shear viscosity to entropy density $\eta/s \sim \hbar/k_B$, and a conductivity that is linear in T [4, 5, 16]. These limiting behaviors can be understood by combining τ_r with a propagation speed $v \sim \sqrt{k_B T/m}$, for example $D \sim v^2 \tau_\mathrm{r}$. This argument applies to ultracold three-dimensional (3D) Fermi gases, whose behavior in the strongly interacting regime is controlled by the quantum critical point at divergent scattering length, zero temperature, and zero density [7, 16–18]. In such systems, one observes $D \gtrsim 2\hbar/m$ [9–11] and $\eta/s \gtrsim 0.4\hbar/k_B$ [6], compatible with conjectured quantum bounds.

However in attractive two-dimensional (2D) Fermi gases, scale invariance is broken by the finite bound-state pair size and the strongly interacting system is no longer controlled by a quantum critical point [17, 19–25]. Strikingly, an extreme violation of one conjectured transport bound has been observed in an ultracold 2D Fermi gas: a spin diffusivity of $6 \times 10^{-3}\hbar/m$ near $\ln(k_\mathrm{F}a_\mathrm{2D}) = 0$ [26], where k_F is the Fermi momentum and a_2D is the 2D s-wave scattering length. No similarly dramatic ef-

fect of dimensionality is observed in charge conductivity [4] or bulk viscosity [20], and such a low spin diffusivity is unexplained by theory [14, 19, 21–24].

In this work, we recreate the conditions of Ref. [26], and study demagnetization dynamics of ultracold 2D Fermi gases using both a coherent spin-echo sequence [11] and time-resolved spectroscopy [10]. We find a modification of the apparent diffusivity by the Leggett-Rice (LR) effect [27] and observe the effects of strong interactions on the thermodynamics of the gas. However, in disagreement with Ref. [26], we find that the quantum bound for the spin diffusivity is satisfied in all conditions accessible to our apparatus.

Our experiments use the three lowest-energy internal states, labeled $|-z\rangle$, $|+z\rangle$, and $|\mathrm{pr}\rangle$, of neutral ^{40}K atoms. Interactions between $|-z\rangle$ and $|+z\rangle$ atoms are tuned by the s-wave Feshbach resonance [29] at 202.1 G, while $|\mathrm{pr}\rangle$ atoms remain weakly interacting with $|\pm z\rangle$ atoms, and any atoms in identical spin states remain non-interacting since the gas is ultracold. An ensemble of 2D systems is prepared by loading a 3D cloud of $|-z\rangle$ atoms into an optical lattice with a period of 380 nm along the x_3 direction [28]. At the final lattice depth of $V_0 = 50\,E_R$, where $E_R/\hbar \simeq 2\pi \times 8.64\,\mathrm{kHz}$, the 2D samples are isolated from one another and in near harmonic confinement with $\omega_3 \simeq 2\pi \times 122\,\mathrm{kHz}$. The transverse confinement with $\omega_{1,2} \simeq 2\pi \times 600\,\mathrm{Hz}$ is controlled by an optical dipole trap. The reduced temperature $(T/T_\mathrm{F})_\mathrm{i}$ of the 2D ensemble can be varied between 0.20 and 1.20, where $T_\mathrm{F} \equiv E_\mathrm{F}/k_B$, and $E_\mathrm{Fi} = \hbar^2 k_\mathrm{Fi}^2/2m$ is the Fermi energy of the central 2D system in its initial polarized state. We parametrize the interaction strength by $\ln(k_\mathrm{Fi}a_\mathrm{2D})$. A static field gradient B' along x_1 is set to $20.3(2)\,\mathrm{G/cm}$
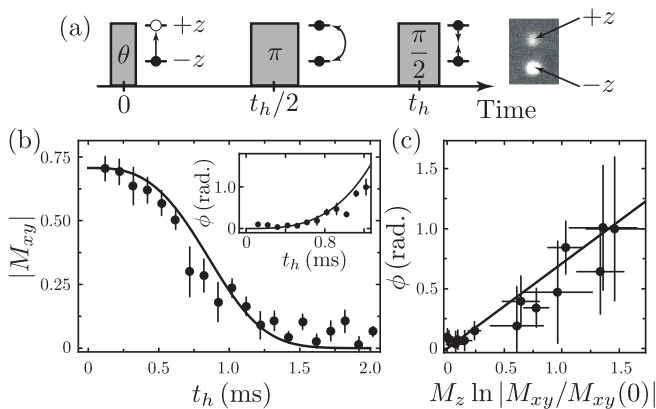
FIG. 1. Magnetization dynamics. (a) The time sequence used to measure the magnetization dynamics is a simple spin-echo sequence which allows us to measure (b) the amplitude and (c) the phase of the ensemble-averaged transverse magnetization. Populations are measured with absorption imaging after Stern-Gerlach separation [28]. γ is found from the slope of $\phi(t_h)$ vs. $M_z \log |M_{xy}/M_{xy}(0)|$. Data is taken with $\theta = 0.25\pi$, leading to $M_z = -0.71$.

unless stated otherwise.

Transport of local magnetization $\boldsymbol{M} = \langle M_x, M_y, M_z \rangle$ occurs through a spin current $\boldsymbol{J}_j$ that can be decomposed into a longitudinal component ($\boldsymbol{J}_j^{\parallel} \parallel \boldsymbol{M}$) and a transverse component ($\boldsymbol{J}_j^{\perp} \perp \boldsymbol{M}$), where bold letters indicate vectors in Bloch space and the subscript $j \in \{1, 2, 3\}$ denotes spatial direction. Our measurements follow a standard spin-echo protocol [30] that initiates a purely transverse current. In the hydrodynamic regime, $\boldsymbol{J}_j^{\perp}$ is the sum of a dissipative term $-D_{\text{eff}}^{\perp} \nabla_j \boldsymbol{M}$ and a reactive term $-\gamma \boldsymbol{M} \times D_{\text{eff}}^{\perp} \nabla_j \boldsymbol{M}$, where $D_{\text{eff}}^{\perp} = D_0^{\perp}/(1 + \gamma^2 M^2)$ is the effective transverse diffusivity, and $D_0^{\perp}$ is the bare diffusivity [27]. The parameter γ quantifies the precession of spin current about the local magnetization, which slows demagnetization – a phenomenon known as the Leggett-Rice effect.

Dynamics are initiated by a resonant radio-frequency (rf) pulse with area θ, which creates a superposition of $|-z\rangle$ and $|+z\rangle$ and thus a magnetization $M_z = -\cos(\theta)$ and $M_{xy} \equiv M_x + iM_y = i\sin(\theta)$. The field gradient causes a twisting of the xy-magnetization into a spiral texture. The gradient in direction of $\boldsymbol{M}$ drives a transverse spin current $\boldsymbol{J}_1^{\perp}$, which tends to relax $M_{xy} \to 0$, while M_z is conserved. These dynamics are described by [27]

$$\partial_t M_{xy} = -i\alpha x_1 M_{xy} + D_{\text{eff}}^{\perp}(1 + i\gamma M_z)\nabla_1^2 M_{xy} \qquad (1)$$

where $\alpha = B'\Delta\mu/\hbar$, and $\Delta\mu$ is the difference in magnetic moment between $|+z\rangle$ and $|-z\rangle$. The solutions of Eq. (1) depend on a dimensionless time $R_M t_h$, where t_h is the total hold time between the initialization pulse and final read out pulse and $R_M \equiv (D_0^{\perp}\alpha^2)^{1/3}$ [28]. In our typical conditions, R_M^{-1} is on the order of 1 ms.

We measure the vector magnetization using a spin-echo

sequence as shown in Fig. 1(a). A π pulse at time $t_h/2$ reverses all M_{xy} phases, so that evolution in the presence of B' causes an untwisting of the spiral magnetization texture. The final $\pi/2$ pulse is applied with a variable phase lag, so that the final populations in $|\pm z\rangle$ can be used to fully characterize the direction $\phi = \arg(M_{xy}/i)$ and the magnitude $|M_{xy}|$ of the transverse magnetization.

Figure 1(b),(c) shows an example of $|M_{xy}(t_h)|$ and $\phi(t_h)$, for an initial pulse angle $\theta = 0.25\pi$. The solution of Eq. (1) for $\gamma \neq 0$ gives $\phi = \gamma M_z \ln |M_{xy}/M_{xy}(0)|$ for all t_h, and thus γ is found by linear regression on data such as Fig. 1(c). Then, R_M (and from it $D_0^{\perp}$) is determined by a nonlinear fit to $|M_{xy}(t_h)|$ data, again using an analytic solution of Eq. (1). $M_{xy}(0) = i\sin(\theta)$ and B' are independently calibrated [28].

For the data shown in Fig. 1, at $\ln(k_{\text{Fi}}a_{2\text{D}}) = 0.13(3)$ and $(T/T_{\text{F}})_{\text{i}} = 0.36(4)$, we find $D_0^{\perp} = 2.3(3)\hbar/m$ and $\gamma = 0.6(1)$. These best-fit transport coefficients are understood as an average both over the ensemble of 2D systems, and over the dynamical changes in the cloud, discussed below. At strong interaction when the mean free path $\sim 1\mu$m is much smaller than the Thomas-Fermi length and the typical minimal spin-helix pitch $\sim 5\mu$m, we expect that the trap averaged transport coefficients are close to the homogeneous values. In this regime the dynamics are essentially local [31].

We search for conditions that minimize $D_0^{\perp}$ by repeating this characterization of $M_{xy}(t_h)$ at various interaction strengths and initial temperatures. Figure 2(a) shows that $D_0^{\perp}$ is smallest when $-0.5 \lesssim \ln(k_{\text{Fi}}a_{2\text{D}}) \lesssim +0.5$, i.e., where $a_{2\text{D}}$ is comparable to k_{F}^{-1}. This condition can be understood by considering the 2D scattering amplitude in vacuum: $f(k) = 2\pi/[-\ln(ka_{2\text{D}}) + i\pi/2]$ [25, 32–34], which gives a maximal (unitary) cross-section $4/k$ at
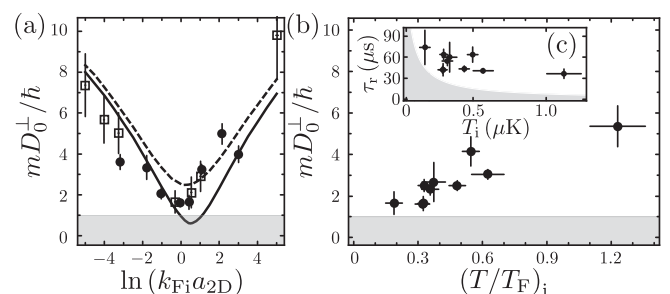

FIG. 2. Transverse spin diffusivity. (a) $D_0^{\perp}$ versus interaction strength with $(T/T_{\text{F}})_{\text{i}} = 0.31(2)$ (black circles) and $(T/T_{\text{F}})_{\text{i}} = 0.21(3)$ (open squares). Each data point corresponds to a complete data set as shown in Fig. 1. The lines are predictions for $T/T_{\text{F}} = 0.3$ by a kinetic theory, as described in the text. (b) $D_0^{\perp}$ versus initial reduced temperature $(T/T_{\text{F}})_{\text{i}}$ at $\ln(k_{\text{Fi}}a_{2\text{D}}) = -0.1(2)$. (c) Local relaxation rate τ_{r} estimated as $D_0^{\perp}/v_T^2$. Shaded regions show $D_0^{\perp} < \hbar/m$ in (a,b), and $\tau_{\text{r}} < \hbar/k_B T$ in (c). Data are consistent with the conjectured quantum bound, which would exclude the shaded areas on all plots.

$ka_{2D} = 1$. Even though our Fermi gas has a distribution of relative momenta k, the average cross-section at low temperature can be estimated by replacement of k with k_F, due to the logarithmic dependence of f on the energy of collision.

The lines on Fig. 2(a) show a kinetic theory both with and without medium scattering (solid and dashed lines, respectively) calculated in the $|\boldsymbol{M}| \to 1$ limit [14, 31]. The model also accounts for inhomogeneities in the following way: first, the collision integral is solved to compute the transverse spin diffusion time and LR parameter for a 2D homogeneous system with the same spin density and temperature as the trap center [14, 35]. Next, these parameters are used to solve the Boltzmann equation for the position-dependent spin density in the full trapping potential for each 2D gas in the ensemble [31]. Finally, the average magnetization dynamics is analyzed using Eq. (1). This procedure predicts a minimal $D_0^\perp$ slightly shifted from the observed minimum; but its results agree well with the increase of $D_0^\perp$ in the weakly interacting regime. This gives us confidence that inhomogeneity effects are well understood.

The lowest observed diffusivity is $D_0^\perp = 1.7(6)\hbar/m$, at $(T/T_F)_i = 0.19(3)$ and $\ln(k_{Fi}a_{2D}) = -0.1(2)$. The effect of temperature is shown in Fig. 2(b) and by data sets in Fig. 2(a) taken at two temperatures. In all cases, our data supports the conjectured bound $D_0^\perp \gtrsim \hbar/m$.

Assuming that spin travels with an average thermal velocity $v_T \sim \sqrt{k_B T/m}$, one can estimate the local relaxation time τ_r with $D_0^\perp/v_T^2$. Figure 2(c) compares this time to the bound $\hbar/k_B T$. Another estimate of the relaxation time might be taken from Fermi liquid theory, which gives $\tau_D = 2(1 + F_0^a)^{-1}D_0/v_F^2$, where v_F is the Fermi velocity, and F_0^a parameterizes magnetic susceptibility [27, 28]. Assuming $(1 + F_0^a)$ is of order unity, and $\tau_r \sim \tau_D$, this would give $\tau_r \sim 20\,\mu s$ at the minimum observed diffusivity, again on the order of $\hbar/k_B T$. In sum, a 2D Fermi gas with $a_{2D}k_F \sim 1$ seems to saturate, but not violate, the Planckian bound $\tau_r^{-1} \lesssim k_B T/\hbar$ at the lowest temperatures probed here.

Figures 3(b) and 3(c) summarize measurements of γ across a wide range of interaction strengths and temperatures. There are two implications of these data. First, system-wide demagnetization is slowed by spin current precession, to an apparent diffusivity $D_{eff}^\perp$, which is initially $D_0^\perp/(1 + \gamma^2)$ for a fully polarized cloud. This is a reasonable quantity to compare to the "$D_s^\perp$" measured in Ref. [26] to be $6.3(8) \times 10^{-3}\hbar/m$ at minimum. In similar conditions, we instead find $D_{eff}^\perp = 7(3) \times 10^{-1}\hbar/m$. In both works, diffusivity is observed to be minimal near $\ln(k_{Fi}a_{2D}) = 0$, and to double between $\ln(k_{Fi}a_{2D}) \approx 0$ and $\ln(k_{Fi}a_{2D}) \approx 1$. However, we cannot explain the hundred-fold difference in scale.

The second implication of γ is to reveal the sign of the interaction between the spin current and the local magnetization [27, 36, 37]. When $\gamma < 0$, as we ob-

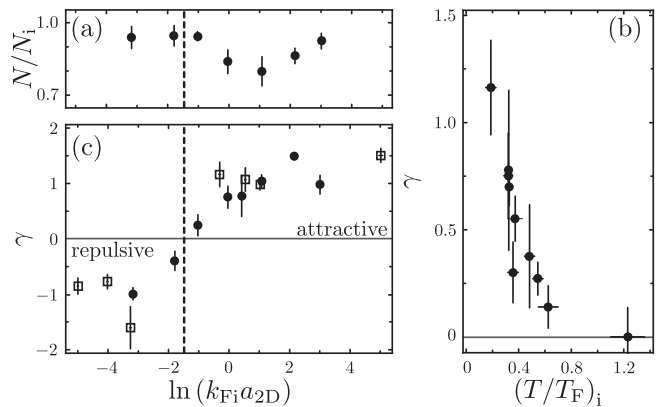FIG. 3. Change in the sign of interaction. (a) Fraction of atoms remaining at $t_h = 3.5\,\text{ms}$. (b) γ versus interaction strength, with markers as in Fig. 2(a). (c) γ versus initial reduced temperature $(T/T_F)_i$, at $\ln(k_{Fi}a_{2D}) = -0.1(2)$. The change in sign of γ, at $\ln(k_{Fi}a_{2D}) \approx -1$, is associated with the onset of a pairing instability.

serve for $\ln(k_{Fi}a_{2D}) \lesssim -1.5$ [see Fig. 3(b)], interactions are repulsive, whereas when $\gamma > 0$, as we observe for $\ln(k_{Fi}a_{2D}) \gtrsim -1$, interactions are attractive. Figure 3(a) shows that above the sign change, some atom loss occurs. These observations indicate that the system is in the *upper energetic branch*, due to its non-equilibrium preparation, distinct from the lower branch in which fermions are paired and form a superfluid at sufficiently low temperature. Unlike in 3D, at the unitarity point in 2D the dimer binding energy is several times E_F, so that an *attractive* upper branch is energetically well defined. The observed onset of the pairing instability agrees with predictions for a quasi-2D Fermi gas with $E_F/\hbar\omega_z = 0.2$ [38], but the instability itself seems weaker than in 3D: at least 80% of the atoms remain after 3.5 ms. This is sufficient to explore spin transport in the metastable upper branch.

One consequence of demagnetization is a cloud-wide redistribution of energy. For a 2D harmonically trapped Fermi gas, the virial relation is [39]

$$V = \frac{1}{2}E + \frac{\hbar^2}{8\pi m}\mathcal{C}_{2D} \qquad (2)$$

where V is the total potential energy, E is the total energy, and $\mathcal{C}_{2D}$ is the (extensive) 2D contact [39, 40]. Since $V = E/2$ for a scale-invariant system, $\mathcal{C}_{2D}$ quantifies the breaking of scale invariance.

In our isolated system E is conserved, however $\mathcal{C}_{2D}$ increases from zero for the non-interacting initial state to a finite positive value for the final state. This implies that V must also increase, which in turn dictates an increase in the rms cloud size: $V/N = \frac{1}{2}m(\omega_1^2\langle x_1^2\rangle + \omega_2^2\langle x_2^2\rangle)$. As a result of the increased $\langle r^2\rangle$, the average density of the cloud must decrease during demagnetization.

Using rf spectroscopy, we measure $\mathcal{C}_{2D}$ throughout the demagnetization dynamics. The experimental protocol is
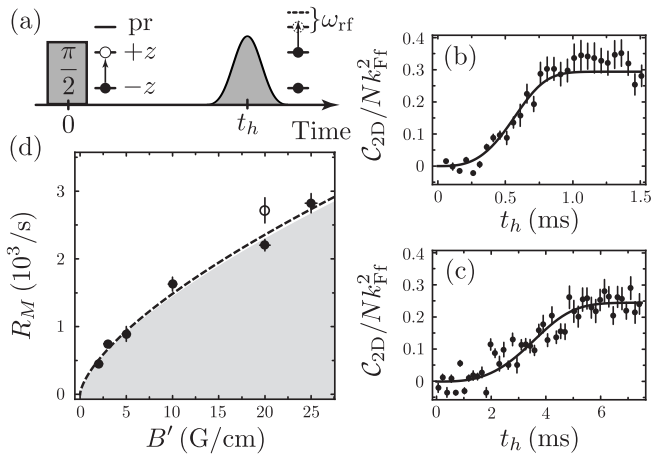
FIG. 4. Contact Dynamics at $\ln(k_{\mathrm{Fi}}a_{2\mathrm{D}}) = 0.35(5)$ and $(T/T_{\mathrm{F}})_{\mathrm{i}} = 0.31(2)$. (a) $\mathcal{C}_{2\mathrm{D}}$ is measured after a hold time t_h by a pulse detuned by ω_{rf} from the $|+z\rangle$-to-$|\mathrm{pr}\rangle$ transition. (b) Contact growth for $B' = 25\,\mathrm{G/cm}$. (c) Contact growth for $B' = 2\,\mathrm{G/cm}$. (d) The best-fit R_M determined from contact growth (black points), versus B'. The shaded region corresponds to R_M with $D_0^{\perp} < \hbar/m$. The open point indicates R_M anticipated from $\boldsymbol{M}$ dynamics at $20\,\mathrm{G/cm}$. The dashed line shows the best fit diffusivity $D_0^{\perp} = 1.1(1)\hbar/m$.

as described in Ref. [10] and depicted in Fig. 4(a). The dynamics are initiated with a $\theta = \pi/2$ pulse and the sample is probed with a spectroscopic pulse that couples the states $|+z\rangle$ and $|\mathrm{pr}\rangle$ after a hold time t_h. The transfer rate of population to state $|\mathrm{pr}\rangle$ is measured as a function of the detuning ω_{rf} from the bare spin-flip resonance, and is known to scale with $\mathcal{C}_{2\mathrm{D}}\omega_{\mathrm{rf}}^{-2}$ in the limit $\omega_{\mathrm{rf}} \gg E_{\mathrm{F}}$ [41–44]. We compensate for final-state interactions between the $|\mathrm{pr}\rangle$ atoms and $|\pm z\rangle$ atoms in our analysis [28, 42].

At $\ln(k_{\mathrm{Ff}}a_{2\mathrm{D}}) = 0.00(5)$ we find that the contact rises from zero to $\mathcal{C}_{2\mathrm{D}}/N = 0.28(3)k_{\mathrm{Ff}}^2$, where $k_{\mathrm{Ff}}^2 = k_{\mathrm{Fi}}^2/2$. Using Eq. (2), one finds $V - E/2 \approx 0.02E_{\mathrm{Ff}}$ per particle, which is a 4% increase on the initial $V/N \approx 0.48E_{\mathrm{F}}$ for a non-interacting gas at $T/T_{\mathrm{F}} = 0.3$. A much larger $\mathcal{C}_{2\mathrm{D}}$ has been found in the lower branch at comparable temperature [44], and $\mathcal{C}_{2\mathrm{D}} \approx 8Nk_{\mathrm{F}}^2$ is expected at $\ln(k_{\mathrm{F}}a_{2\mathrm{D}}) = 0$ [45]. We note that without the mean-field dimer contribution $\mathcal{C}_0$ to the contact, the remaining "many-body contact" $\mathcal{C}_{2\mathrm{D}} - \mathcal{C}_0$ in the lower branch is however comparable to our observations: peak extensive $\mathcal{C}_{2\mathrm{D}} - \mathcal{C}_0$ is roughly $0.3Nk_{\mathrm{F}}^2$ [45]. Since the contact is also a measure of two-body correlations at short range, this suggest that the upper branch is as strongly correlated as the lower branch, even though the virial is relatively weakly modified.

A final thermodynamic transformation accompanying demagnetization is a temperature rise due to the combination of increased spin entropy and decreased occupation of the Fermi sea [46]. For an initial temperature of $0.3(1)\,T_{\mathrm{Fi}}$ and a $\pi/2$ pulse, we observe $T_{\mathrm{f}} = 0.7(2)\,T_{\mathrm{Ff}}$ near $\ln(k_{\mathrm{Ff}}a_{2\mathrm{D}}) = 0$. Due to the released attractive in-

teraction energy, this temperature rise is larger than the $\Delta(T/T_{\mathrm{F}}) \approx 0.25$ one would expect from demagnetization of an ideal gas. However the observed heating is three times smaller than the $\Delta(T/T_{\mathrm{F}}) \approx 2.2$ that is predicted using the equilibrium 2D equation of state [45, 47, 48] for thermalization to the lower branch. This further supports the interpretation that the 2D gas remains predominantly in the upper branch during demagnetization.

Figures 4(b),(c) show the typical dynamics we observe when measuring $\mathcal{C}_{2\mathrm{D}}(t_h)$ at $\ln(k_{\mathrm{Fi}}a_{2\mathrm{D}}) = 0.35(5)$. Due to Pauli exclusion, we can use such data to infer magnetization dynamics: pairs of fermions must have a singlet wave function to interact through an s-wave contact interaction. The singlet fraction can be no larger than $1 - |\boldsymbol{M}|$, and would be $(1 - |\boldsymbol{M}|^2)/4$ for uncorrelated spins [10, 49, 50]. For the $\pi/2$ initialization pulse performed here, $|\boldsymbol{M}| = |M_{xy}|$ since $M_z = 0$. A direct comparison between $\boldsymbol{M}$ and $\mathcal{C}_{2\mathrm{D}}$ at $B' = 20\,\mathrm{G/cm}$ (see [28]) shows a correlation that lies between these two limits: $\mathcal{C}_{2\mathrm{D}}/N$ is proportional to $1 - |M_{xy}(t_h)|^{1.4(2)}$. This form with $\gamma = 0.71$ is used to fit $\mathcal{C}_{2\mathrm{D}}$ data for a variety of gradients [see Fig. 4(b),(c)] and extract R_M.

Across the experimentally accessible gradients B', Fig. 4(d) shows a range of R_M from $4.4(2) \times 10^2\,\mathrm{s}^{-1}$ to $2.9(2) \times 10^3\,\mathrm{s}^{-1}$. Throughout, R_M scales with $\alpha^{2/3}$ (see dashed line) and can be explained by a single diffusivity $D_0^{\perp} = 1.1(1)\hbar/m$. This verifies that the microscopic $D_0^{\perp}$ is independent of B' across the accessible range, and thus independent of the pitch of the spin helix. The comparable magnitude of $D_0^{\perp}$ determined by two measurement techniques is also a reassuring check on the fidelity of the spin-echo sequence used in $\boldsymbol{M}$ measurements, since the measurement of $\mathcal{C}_{2\mathrm{D}}$ does not rely upon successful rephasing of the spins at the echo time.

In sum, we have observed quantum-limited spin transport in strongly interacting 2D Fermi gases. We find that the conjectured lower bound $D_0^{\perp} \gtrsim \hbar/m$ is respected for all interaction strengths, temperatures, and applied field gradients accessible to our apparatus. At the lowest temperatures measured, and when $k_{\mathrm{F}}a_{2\mathrm{D}}$ is comparable to unity, diffusivity saturates the quantum bound, which implies that the system is "Planckian", with a local relaxation rate $\tau_{\mathrm{r}}^{-1} \sim k_BT/\hbar$. Even though not in the class of quantum critical systems, 2D transport dynamics are similar to those in 3D due to an apparent scale invariance in the strong coupling regime, because corrections to the unitary scattering cross section are only logarithmic [19, 22–24, 42], and because dimers play no significant role during demagnetization.

[1] P. K. Kovtun, D. T. Son, and A. O. Starinets, Phys. Rev. Lett. **94**, 111601 (2005); A. Adams, L. D. Carr, T. Schäfer, P. Steinberg, and J. E. Thomas, New J Phys **14**, 115009 (2012); T. Schäfer and D. Teaney, Rep. Prog. Phys. **72**, 126001 (2009).

[2] H. Song, Nuclear Physics A **904**, 114c (2013).

[3] M. Müller, J. Schmalian, and L. Fritz, Phys. Rev. Lett. **103**, 025301 (2009).

[4] J. A. N. Bruin, H. Sakai, R. S. Perry, and A. P. Mackenzie, Science **339**, 804 (2013).

[5] S. A. Hartnoll, Nat Phys **11**, 54 (2015).

[6] C. Cao, E. Elliott, J. Joseph, H. Wu, J. Petricka, T. Schäfer, and J. E. Thomas, Science **331**, 58 (2011); E. Elliott, J. A. Joseph, and J. E. Thomas, Phys. Rev. Lett. **113**, 020406 (2014); J. A. Joseph, E. Elliott, and J. E. Thomas, Phys. Rev. Lett. **115**, 020401 (2015).

[7] T. Enss, R. Haussmann, and W. Zwerger, Annals of Physics **326**, 770 (2011); T. Enss, Phys. Rev. A **86**, 013616 (2012).

[8] G. Wlazłowski, P. Magierski, and J. E. Drut, Phys. Rev. Lett. **109**, 020406 (2012); G. Wlazłowski, W. Quan, and A. Bulgac, Phys. Rev. A **92**, 063628 (2015).

[9] A. Sommer, M. Ku, G. Roati, and M. W. Zwierlein, Nature **472**, 201 (2011).

[10] A. B. Bardon, S. Beattie, C. Luciuk, W. Cairncross, D. Fine, N. S. Cheng, G. J. A. Edge, E. Taylor, S. Zhang, S. Trotzky, and J. H. Thywissen, Science **344**, 722 (2014).

[11] S. Trotzky, S. Beattie, C. Luciuk, S. Smale, A. B. Bardon, T. Enss, E. Taylor, S. Zhang, and J. H. Thywissen, Phys. Rev. Lett. **114**, 015301 (2015).

[12] G. M. Bruun, New J. Phys. **13**, 035005 (2011); G. M. Bruun and C. J. Pethick, Phys. Rev. Lett. **107**, 255302 (2011).

[13] D. Wulin, H. Guo, C.-C. Chien, and K. Levin, Phys. Rev. A **83**, 061601 (2011); M. P. Mink, V. P. J. Jacobs, H. T. C. Stoof, R. A. Duine, M. Polini, and G. Vignale, Phys. Rev. A **86**, 063631 (2012); H. Heiselberg, Phys. Rev. Lett. **108**, 245303 (2012); H. Kim and D. A. Huse, Phys. Rev. A **86**, 053607 (2012); O. Goulko, F. Chevy, and C. Lobo, New J. Phys. **14**, 073036 (2012); T. Enss and R. Haussmann, *ibid.* **109**, 195303 (2012).

[14] T. Enss, Phys. Rev. A **88**, 033630 (2013).

[15] J. Zaanen, Nature **430**, 512 (2004).

[16] S. Sachdev, *Quantum Phase Transitions*, 2nd ed. (Cambridge, 2011).

[17] P. Nikolic and S. Sachdev, Phys. Rev. A **75**, 033608 (2007).

[18] M. Y. Veillette, D. E. Sheehy, and L. Radzihovsky, Phys. Rev. A **75**, 043614 (2007).

[19] J. Hofmann, Phys. Rev. A **84**, 043603 (2011).

[20] E. Vogt, M. Feld, B. Fröhlich, D. Pertot, M. Koschorreck, and M. Köhl, Phys. Rev. Lett. **108**, 070404 (2012).

[21] G. M. Bruun, Phys. Rev. A **85**, 013636 (2012).

[22] T. Schäfer, Phys. Rev. A **85**, 033623 (2012).

[23] T. Enss, C. Küppersbusch, and L. Fritz, Phys. Rev. A **86**, 013617 (2012).

[24] E. Taylor and M. Randeria, Phys. Rev. Lett. **109**, 135301 (2012).

[25] J. Levinsen and M. Parish, Ann. Rev. Cold Atoms Mols. **3**, 1 (2015).

[26] M. Koschorreck, D. Pertot, E. Vogt, and M. Köhl, Nature Phys. **9**, 405 (2013).

[27] A. J. Leggett and M. J. Rice, Phys. Rev. Lett. **20**, 586 (1968); A. J. Leggett, J. Phys. C **3**, 448 (1970).

[28] See Supplemental Material for further details of experimental and theoretical methods.

[29] C. Chin, R. Grimm, P. Julienne, and E. Tiesinga, Rev. Mod. Phys. **82**, 1225 (2010).

[30] E. L. Hahn, Phys. Rev. **80**, 580 (1950); H. Y. Carr and E. M. Purcell, Phys. Rev. **94**, 630 (1954); H. C. Torrey, Phys. Rev. **104**, 563 (1956).

[31] T. Enss, Phys. Rev. A **91**, 023614 (2015).

[32] J. R. Engelbrecht, M. Randeria, and L. Zhang, Phys. Rev. B **45**, 10135 (1992).

[33] D. S. Petrov and G. V. Shlyapnikov, Phys. Rev. A **64**, 012706 (2001).

[34] I. Bloch, J. Dalibard, and W. Zwerger, Reviews of Modern Physics **80**, 885 (2008).

[35] J. W. Jeon and W. J. Mullin, Phys. Rev. Lett. **62**, 2691 (1989).

[36] C. Lhuillier and F. Laloë, J. Phys.-Paris **43**, 225 (1982).

[37] K. Miyake, W. J. Mullin, and P. C. E. Stamp, J Phys-Paris **46**, 663 (1985).

[38] V. Pietilä, D. Pekker, Y. Nishida, and E. Demler, Phys. Rev. A **85**, 023621 (2012).

[39] M. Valiente, N. T. Zinner, and K. Mølmer, Phys. Rev. A **84**, 063626 (2011).

[40] S. Tan, Ann. Phys. **323**, 2987 (2008); E. Braaten and L. Platter, Phys. Rev. Lett. **100**, 205301 (2008); S. Zhang and A. J. Leggett, Phys. Rev. A **79**, 023601 (2009); R. Combescot, F. Alzetto, and X. Leyronas, Phys. Rev. A **79**, 053640 (2009); F. Werner and Y. Castin, Phys. Rev. A **86**, 013626 (2012).

[41] E. Braaten, D. Kang, and L. Platter, Phys. Rev. Lett. **104**, 223004 (2010).

[42] C. Langmack, M. Barth, W. Zwerger, and E. Braaten, Phys. Rev. Lett. **108**, 060402 (2012).

[43] W. Schneider and M. Randeria, Phys. Rev. A **81**, 021601 (2010).

[44] B. Fröhlich, M. Feld, E. Vogt, M. Koschorreck, M. Kohl, C. Berthod, and T. Giamarchi, Phys. Rev. Lett. **109**, 130403 (2012).

[45] G. Bertaina and S. Giorgini, Phys. Rev. Lett. **106**, 110403 (2011); M. Bauer, M. M. Parish, and T. Enss, Phys. Rev. Lett. **112**, 135302 (2014); H. Shi, S. Chiesa, and S. Zhang, Phys. Rev. A **92**, 033603 (2015); E. R. Anderson and J. E. Drut, Phys. Rev. Lett. **115**, 115301 (2015); A. Galea, H. Dawkins, S. Gandolfi, and A. Gezerlis, Phys. Rev. A **93**, 023602 (2016).

[46] R. Ragan, K. Grunwald, and C. Glenz, J. Low Temp Phys **126**, 163 (2002).

[47] K. Fenech, P. Dyke, T. Peppler, M. G. Lingham, S. Hoinka, H. Hu, and C. J. Vale, Phys. Rev. Lett. **116**, 045302 (2016).

[48] I. Boettcher, L. Bayha, D. Kedar, P. A. Murthy, M. Neidig, M. G. Ries, A. N. Wenz, G. Zürn, S. Jochim, and T. Enss, Phys. Rev. Lett. **116**, 045303 (2016).

[49] G. S. Thekkadath, L. Jiang, and J. H. Thywissen, J Phys B-At Mol Opt **49**, 1 (2016).

[50] W.-B. He, Y.-Y. Chen, S. Zhang, and X.-W. Guan, Phys. Rev. A **94**, 031604 (2016).

SUPPLEMENTARY MATERIAL

Sample preparation. We sympathetically cool fermionic spin-polarized ^{40}K using bosonic ^{87}Rb. Initially both species are trapped in a microfabricated magnetic chip trap where ^{87}Rb undergoes forced rf evaporative cooling. Subsequently both species are loaded into a crossed-beam optical dipole trap with aspect ratio 6:1:1 where an additional stage of evaporative cooling with variable end point determines the initial number and temperature of the sample. A resonant light pulse removes any remaining ^{87}Rb leaving a spin-polarized degenerate Fermi gas, typically with $N \approx 4 \times 10^4$ atoms at a temperature $T \approx 150$ nK in the lowest hyperfine state of the electronic ground state. The $|-z\rangle$, $|+z\rangle$, and $|\mathrm{pr}\rangle$ states in the main text refer to the high-field states adiabatically connected to the low-field $m_f = -9/2, -7/2,$ and $-5/2$ states of the $f = 9/2$ hyperfine manifold, where f and m_f refer to the total angular momentum and corresponding magnetic quantum number, respectively.

Our 3D sample is adiabatically loaded into a one dimensional optical lattice formed from a standing wave of 760.2 nm light with corresponding recoil energy $E_R/\hbar = 2\pi \times 8.64$ kHz. The lattice depth V_0 is ramped up in two stages: first to approximately 5 E_R in 100 ms where the tunneling between adjacent sites is effectively frozen out, and then in 5 ms to 50 E_R where we perform our experiments. The final lattice depth is determined using amplitude modulation spectroscopy to resonantly create excitations from the ground band to the second excited band of the lattice which we observe as population in the second Brillouin zone after band-mapping.

This loading procedure typically populates two hundred planes with radial trapping frequency $\omega_{1,2} = 2\pi \times 600(35)$ Hz and tight transverse confinement $\omega_3 = 2\pi \times 122(35)$ kHz. In the central 2D gas we typically have 500 atoms with a global initial Fermi energy $E_{\mathrm{Fi}} = \hbar\omega_{1,2}(2N)^{1/2} \approx h \times 19$ kHz, well within the 2D regime ($E_F \ll \hbar\omega_3$).

Temperature control and determination. We vary the temperature of our ensemble of 2D gases by varying the initial temperature before loading the optical lattice. This is accomplished by changing the final trap depth during evaporation in the dipole trap. Given the initial temperature, number and trap parameters we simulate the final temperature expected in the lattice.

Adiabatic loading into the optical lattice increases the temperature due to the modified density of states: for a 3D cloud prepared with $T/T_F \simeq 0.15$, we observe an average $T/T_F \simeq 0.20$ for the 2D clouds, which agrees with a calculation that assumes adiabatic loading. In the main text the Fermi temperature $T_F = E_F/k_B$ where E_F is the Fermi energy of the central 2D system.
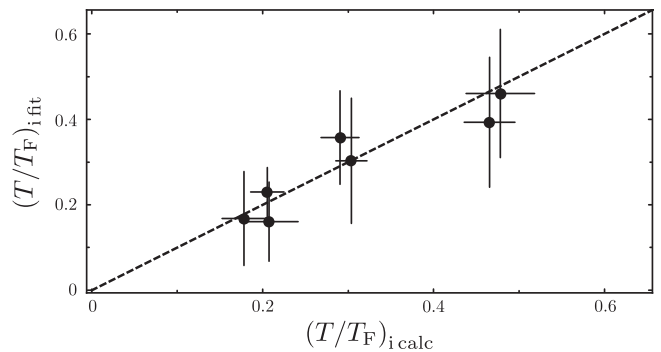
The optical lattice modifies the harmonic potential the

FIG. S1. Thermometry. A comparison of the fitted temperature $(T/T_F)_{\mathrm{i\,fit}}$ and calculated ensemble average temperature $(T/T_F)_{\mathrm{i\,calc}}$. The vertical error bars show statistical uncertainty from 10-20 images. The dashed line has a slope of unity.

atoms are initially confined in. This leads to a shift in the ground state energy of each lattice site by an amount $E_j = m\omega_c^2(js)^2/2$ where j labels the lattice site, s is the spacing between sites, and ω_c is the trapping frequency in the 3-direction in the combined potential of the lattice and dipole trap. This introduces a new density of states in the lattice direction and gives a modified density of states for the combined harmonic potential and lattice. To determine the final number and temperature in the lattice we assume isentropic loading and population in only the ground band (as verified by band-mapping). We match the entropy in the 3D harmonic trap with the entropy in the combined system to determine the fugacity in the combined system. For each lattice site we then calculate the fugacity and use this to determine the reduced temperature and number. Figure S1 shows that the temperature predicted using this model is consistent the measured temperature after time-of-flight.

In the main text, we use the calculated temperature to define the initial reduced temperature $(T/T_F)_{\mathrm{i}}$, where $T_{\mathrm{Fi}} = E_{\mathrm{Fi}}/k_B$, and the initial Fermi wave vector k_{Fi}. Uncertainty in $(T/T_F)_{\mathrm{i}}$ is determined by repeating the calculation for initial numbers and temperatures normally distributed around the mean values determined from fitting a 3D Fermi-Dirac distribution to following time-of-flight images of the gas is released from the dipole trap (before the lattice is ramped on). The widths of the distributions include both the shot-to-shot fluctuations and the drift in number and temperature before and after a data set (approximately 3 hours).

Field and gradient control. We control the magnetic field and its gradients using a combination of magnetic field coils and wires on the atom chip $\approx 200\mu m$ from the atoms. We tune the field $|\mathbf{B}|$ near 202.1 G where the states $|\pm z\rangle$ undergo a magnetic Feshbach resonance. We stabilize the field to about 1 part in 10^5. We calibrate the field by measuring the $|-z\rangle$ to $|+z\rangle$ transition frequency and converting the frequency to magnetic field

using the Breit-Rabi formula. During a measurement the field drifts by as much as 0.02 G which, when combined with the number and temperature uncertainty, gives an uncertainty in $\ln(k_F a_{2D})$ of 0.04.

We vary the gradient $B' = |\langle \nabla_1 B, \nabla_2 B, \nabla_3 B \rangle|$ by changing the sum and difference of currents through parallel wires on the atom chip. Unless otherwise stated in the main text, we choose a gradient of $\nabla_1 B = 20.3(2)$ G/cm and $\nabla_2 B = 0.3(6)$ G/cm measured by repeating spectroscopy measurements on a cloud translated by piezo-actuated mirrors on the trapping beams. There is a residual gradient $\nabla_3 B \approx -2.7$ G/cm that we cannot control, however, this is in the same direction as the tight confinement and does not contribute to the demagnetization dynamics.

Imaging. Our imaging scheme allows us to count the population of atoms in two of the three states discussed. For the demagnetization dynamics we image atoms in states $|-z\rangle$ and $|+z\rangle$, while for the spectroscopy measurements we image atoms in states $|+z\rangle$ and $|pr\rangle$. We achieve this population counting by applying a Stern-Gerlach pulse to separate the trapped spin states, rf state manipulation during time-of-flight in a residual gradient, and finally absorption imaging of the $|f = 9/2, m_f = -9/2\rangle$ to $|f' = 11/2, m'_f = -11/2\rangle$ cycling transition.

Fitting of magnetization dynamics. We measure the magnetization decay for various initial amplitudes of the transverse magnetization $|M_{xy}(0)| = \sin\theta$ using a $\theta - \pi - \pi/2$ pulse sequence. To minimize the duration of data sets we fix $\theta \approx 0.25\pi$ calibrated by optimizing a π pulse and then decreasing the duration of the pulse by $1/4$. The first two pulses have the same phase while the last pulse has a variable relative phase lag. An oscillation in the population is generated by varying the phase lag from which the magnitude $|M_{xy}|$ and phase $\phi = -\arg(iM_{xy})$ of the transverse magnetization can be measured. We determine the amplitude and phase of the transverse magnetization from a sinusoidal fit to this oscillation.

We are sensitive to the relative frequency between the drive and the atomic frequency with a precision of $\sim 1/t_h$, where t_h is the hold time. For $t_h \geq 1.5$ ms we find that our field stability is insufficient to produce a reproducible phase, and thus to determine γ or the bare $D_0^\perp$. To avoid this, we work at a sufficiently high magnetic field gradient that the demagnetization time is less than 1.5 ms. As described in the main text, lower field gradients are explored using $\mathcal{C}_{2D}$ dynamics, which is insensitive to uniform field fluctuations.

For each data set $\{|M_{xy}(t_h)|, \phi(t_h)\}$ we determine $D_0^\perp$

and γ using the solution to Eq. (1) given by

$$|M_{xy}(t_h)| = |M_{xy}(0)|\sqrt{\frac{1}{\eta}\mathcal{W}\left(\eta \exp\left[\eta - \frac{(R_M t_h)^3}{6(1 + \gamma^2 M_z^2)}\right]\right)}$$

$$\phi(t_h) = \gamma M_z \ln\left(\frac{|M_{xy}(t_h)|}{|M_{xy}(0)|}\right) \tag{S1}$$

where $\alpha = B'\Delta\mu/\hbar$, $\eta = \gamma^2|M_{xy}(0)|^2/(1 + \gamma^2 M_z^2)$, and $\mathcal{W}(z)$ is the Lambert-W function. The characteristic time scale for the dynamics is $R_M^{-1} \equiv (D_0^\perp \alpha^2)^{-1/3}$. We plot $\phi(t_h)$ versus $M_z \ln(|M_{xy}(t_h)|/|M_{xy}(0)|)$ as in Fig. 1(c) of the main text. A linear fit to this data determines γ. We then fix γ and fit $|M_{xy}(t_h)|$ to determine $D_0^\perp$. After determination of γ, the only effect of $D_0^\perp$ is to rescale time; in other words, for a fixed γ, Eq. (S1) is a universal function of $R_M t_h$, for all $D_0^\perp$, α, and t_h.

Fermi liquid theory in 2D. For a dilute, weakly repulsive Fermi gas in two dimensions, the ground state is a stable Fermi liquid [32] and the Landau interaction f function is given to second order in the coupling $g = -1/\ln(k_F a_{2D})$ by

$$F^s(\theta) = g + g^2\left(2 + \ln\left|\cos\frac{\theta}{2}\right|\right) \tag{S2}$$

$$F^a(\theta) = -g - g^2 \ln\left|\cos\frac{\theta}{2}\right|. \tag{S3}$$

The first angular Fourier coefficients defined by $F^{s,a}(\theta) = \sum_m F_m^{s,a} e^{im\theta}$ are

$$F_0^s = g + g^2(2 - \ln 2), \qquad F_1^s = g^2/2, \tag{S4}$$

$$F_0^a = -g + g^2 \ln 2, \qquad F_1^a = -g^2/2. \tag{S5}$$

The effective mass $m^*/m = 1 + F_1^s = 1 + g^2/2$ and the spin susceptibility $\chi/\chi_0 = (1 + F_1^s)/(1 + F_0^a) = 1 + g + g^2(3/2 - \ln 2)$. The transverse spin diffusivity in 2D at
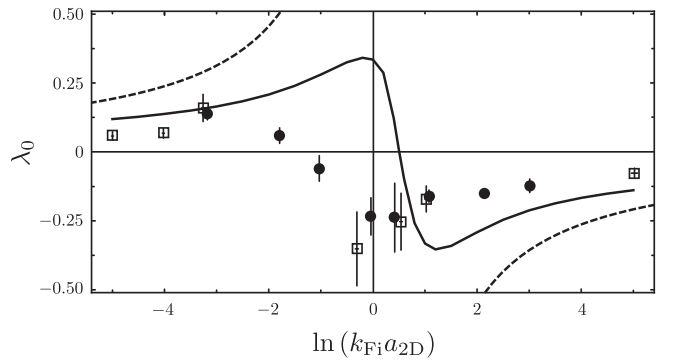

FIG. S2. Comparison to FLT. The effective interaction λ_0 is plotted for a range of temperatures and interaction strengths. Data points show $\lambda_0 = -\hbar\gamma/(2mD_0^\perp)$ for $(T/T_F)_i = 0.31(2)$ (black circles) and $(T/T_F)_i = 0.21(3)$ (open squares). Dashed lines show λ predicted by weak coupling theory, Eq. (S12); solid lines show a $\mathcal{T}$-matrix calculation for the trapped gas.

low temperature is given by

$$D_0^\perp = \frac{\chi_0}{\chi}\frac{\tau_\perp \varepsilon_{\rm F}}{m^*} = (1 + F_0^{\rm a})\frac{\tau_D v_{\rm F}^2}{2}, \tag{S6}$$

where $v_{\rm F}$ is the Fermi velocity, or conversely the transverse scattering time is

$$\tau_D = \frac{2D_0^\perp}{v_{\rm F}^2(1 + F_0^{\rm a})}. \tag{S7}$$

The spin-rotation parameter can be written in terms of the scattering time and a mean-field interaction W between unlike spins [31],

$$\gamma = -\frac{\tau_D W n}{\hbar}. \tag{S8}$$

Following the notation in [11], the relation of γ to the parameter μ used in the liquid ^{3}He literature is $\gamma = n\mu/2$ where n is the total number density.

The ratio $\gamma/D_0^\perp$ eliminates the scattering time and allows one to define the dimensionless effective interaction λ in terms of the measured quantities γ and $D_0^\perp$,

$$\lambda = -\frac{\hbar\gamma}{2m^* D_0^\perp}. \tag{S9}$$

From the definition of the mean-field interaction W [31] one can express λ in terms of the Landau parameters,

$$\lambda = \frac{g(0)W}{1 + F_0^{\rm a}} = \frac{1}{1 + F_0^{\rm a}} - \frac{1}{1 + F_1^{\rm a}} \tag{S10}$$

where $g(0)$ denotes the density of states per spin state. To second order in the perturbative weak-coupling expansion (S5) we find

$$\lambda = g - g^2(\ln 2 - 1/2) + \mathcal{O}(g^3) \tag{S11}$$
$$= -\frac{1}{\ln(k_{\rm F}a_{\rm 2D}) - (\ln 2 - 1/2)} + \mathcal{O}(|\ln(k_{\rm F}a_{\rm 2D})|^{-3}). \tag{S12}$$

The divergence near $\ln(k_{\rm F}a_{\rm 2D}) = \ln 2 - 1/2 \approx 0.2$ signals the breakdown of the perturbative expansion. The true solution should exhibit a zero crossing as the interacting gas crosses over from effective repulsive interactions $\lambda > 0$ at $\ln(k_{\rm F}a_{\rm 2D}) \lesssim -1$ to effective attractive interactions $\lambda < 0$ at $\ln(k_{\rm F}a_{\rm 2D}) \gtrsim 1$.

Figure S2 compares the FLT prediction of λ, the full $\mathcal{T}$-matrix calculation of λ, and the measured values of $\lambda_0 = (m^*/m)\lambda$ (which needs no knowledge of mass renormalization). Near $\ln(k_{\rm Fi}a_{\rm 2D}) \approx 0.2$, both experiment and the full $\mathcal{T}$-matrix calculation give a finite value in contrast to the divergence predicted by the weak-coupling expansion. We note that in the data $\lambda_0 \sim -0.4$ at peak, nearly twice as large as in 3D [11].

Dimer binding energy. Since we create a quasi-2D system by strong out-of-plane confinement, the dimer binding energy $\hbar^2/ma_{\rm 2D}^2$ is determined by 2D physics only for $\ell/a \lesssim -1$, where $a_{\rm 2D} \approx \ell\sqrt{\pi/B}\exp[-\sqrt{\pi/2}\ell/a]$, $B \approx 0.905$, $\ell^2 = \hbar/m\omega_3$, and a is the 3D scattering length. For $\ell/a \gtrsim 1$, dimers are three-dimensional and have a binding energy $\approx \hbar\omega_3 + \hbar^2/ma^2$ [25, 33, 34].

Final state corrections in spectroscopy. The high-frequency tail in the spectral density $I_\sigma(\omega_{\rm rf})$ of the rf transition to a non-interacting probe state ($\int I_\sigma(\omega_{\rm rf})d\omega_{\rm rf} = N_\sigma$) is given by [43]

$$I_\sigma(\omega_{\rm rf}) \to \frac{1}{4\pi}\mathcal{C}_{\rm 2D}\left(\frac{\hbar}{m}\right)\omega_{\rm rf}^{-2}. \tag{S13}$$

where $\omega_{\rm rf}$ is the detuning from resonance and $\mathcal{C}_{\rm 2D}$ is the 2D contact. Following the convention of [10] we introduce the normalized dimensionless detuning $\Delta \equiv \hbar\omega_{\rm rf}/E_{\rm F}$ and normalized transfer rate $\widetilde{\Gamma} \equiv E_{\rm F}I_\sigma/(2\hbar N_\sigma)$ which obeys the sum rule $\int \widetilde{\Gamma}(\Delta)d\Delta = 1/2$ where we have identified $I_\sigma = 2N_p/(\Omega_R^2\pi t_{\rm rf})$. Here Ω_R is the Rabi frequency and $t_{\rm rf}$ is the duration of the rf pulse. Combining this normalization with Eq. (S13) and taking final state interactions into account [42, 44], for $\Delta \gg 1$, we have

$$\widetilde{\Gamma} \to \frac{1}{2\pi}\frac{\mathcal{C}_{\rm 2D}}{Nk_{\rm F}^2}\Delta^{-2} \times \frac{\ln^2(\widetilde{E}_B/E_B)}{\ln^2(\Delta E_{\rm F}/\widetilde{E}_B) + \pi^2} \tag{S14}$$

where $\widetilde{E}_B$ is the binding energy of the most weakly bound state of atoms in the final state and E_B is the binding energy of the confinement induced dimer. For spectroscopic measurements we use the definition $k_{\rm Ff} = k_{\rm F,mix}$. We use Eq. (S14) to determine $\mathcal{C}_{\rm 2D}(t_h)/(Nk_{\rm Ff}^2)$. The time-resolved data in Fig. 4 of the main text is taken at a single frequency $\Delta = 9.5$.

Figure S3 shows a representative spectrum at $\ln(k_{\rm Fi}a_{\rm 2D}) = 0.35(5)$ before and after accounting for final state interactions. We ensure that an appropriate Rabi frequency is chosen such that for $\Delta \gtrsim 5$ (where we extract a value of $\mathcal{C}_{\rm 2D}$) we probe the transition in the linear regime.
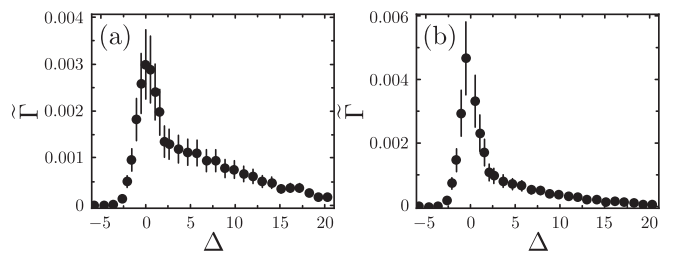

FIG. S3. Spectroscopy. (a) A typical spectrum taken at $\ln(k_{\rm Fi}a_{\rm 2D}) = 0.35(5)$ after normalization. (b) The same spectrum after rescaling to account for final state interactions using Eq. (S14).

Direct comparison of contact and magnetization dynamics. In order to compare $\mathcal{C}_{2D}$ and M_{xy} dynamics a spin-refocussing π pulse can be applied to the $\mathcal{C}_{2D}$ measurement described in the main text at time $t_h/2$. The evolution of $\mathcal{C}_{2D}$ with a spin-refocussing pulse is a factor $4^{-1/3}$ slower than without and otherwise identical. Comparing to a $1 - |M|^{\beta}$ dependence, we find our data fall somewhere between the fully correlated $\beta = 1$ and fully uncorrelated $\beta = 2$ limits. A fit to a $1 - |M|^{\beta}$ dependence finds $\beta = 1.4(2)$. We use this value of β to model the dynamics of $\mathcal{C}_{2D}$.